Journal of
Materials Chemistry B

Materials for biology and medicine

Accepted Manuscript

This article can be cited before page numbers have been issued, to do this please use: S. Wan, D. Esrafilzadeh, L. A. Poole-Warren, K. Kilian and U. A. Aregueta Robles, *J. Mater. Chem. B*, 2026, DOI: 10.1039/D5TB02475G.

ROYAL SOCIETY OF CHEMISTRY

rsc.li/materials-b

View Article Online
DOI: 10.1039/D5TB02475G

Poly-L-Lysine integration in PVA hydrogels enables stable, bioactive matrices for motor neuron differentiation and neural network formation

Shuqian Wan[1], Dorna Esrafilzadeh[1], Laura Poole-Warren[1,2], Kristopher A. Kilian[3,4],

Ulises Aregueta Robles[1]

[1]School of Biomedical Engineering, The University of New South Wales, Sydney, NSW 2052, Australia

[2]Tyree Foundation Institute of Health Engineering, The University of New South Wales, Sydney, NSW 2052, Australia

[3]School of Chemistry, Australian Centre for NanoMedicine, The University of New South Wales, Sydney, NSW 2052, Australia

[4]School of Materials Science and Engineering, The University of New South Wales, Sydney, NSW 2052, Australia

Abstract

The regeneration of motor neurons remains a major challenge in neural tissue engineering due to the complex cellular architecture and dynamic microenvironment of neural systems. While three-dimensional (3D) hydrogels offer a promising biomimetic platform, the stable integration of bioactive molecules such as laminin is hindered by high cost and impact on structural stability. Poly-L-lysine (PLL), commonly employed in 2D systems to enhance cell adhesion and laminin retention, faces critical limitations in 3D applications, including undefined optimal dosing, cytotoxicity at high concentrations, and detrimental effects on hydrogel properties. In this study, we developed a stable, biocompatible poly (vinyl alcohol) (PVA)-based hydrogel incorporating PLL via either physical entrapment (blended PVA-PLL) or covalent methacrylation (covalent PVA-PLL). Systematic optimization identified a minimal effective PLL concentration (0.002 wt%) that enhanced laminin retention and motor neuron progenitors (MNPs) adhesion without inducing cytotoxicity or compromising hydrogel stability. Notably, covalent PLL-MA incorporation provided no significant advantage over physical adsorption at this low concentration, streamlining hydrogel fabrication. A cluster-based morphometric analysis further confirmed superior cell adhesion, neurite outgrowth,

View Article Online
DOI: 10.1039/D5TB02475G

and early network formation on PLL-integrated hydrogels relative to 2D controls. This work established PLL as a simple, scalable, and effective modulator for improving cell adhesion and bioactivity in 3D neural scaffolds, offering translational potential for motor neuron regeneration in spinal cord injury and neurodegenerative disease models.

Keywords: Neural tissue engineering, hydrogel, poly-L-lysine, cell adhesion, laminin retention

1. Introduction

Engineering in vitro neural tissue models requires biomaterials capable of presenting biochemical cues in stable 3D structures. For this purpose, hydrogels are promising 3D platforms offering tissue-mimicking substrates through diverse natural and synthetic materials. Natural hydrogels inherently contain extracellular matrix (ECM) proteins such as laminin, essential for promoting neural cell adhesion, neurite extension, and differentiation[1]. However, their variability and limited stability restrict reproducibility and long-term use. This limitation has driven interest in biosynthetic systems that integrate complex ECM proteins within synthetic hydrogel networks, but such approaches can disrupt hydrogel architecture, limiting biocompatibility, and long-term stability. Poly-L-lysine (PLL) has long been established in 2D cultures as an intermediary molecule for presenting neurons with laminin (LN) to support cell adhesion[2, 3]. Recently, synthetic hydrogels have been functionalized with PLL for

View Article Online
DOI: 10.1039/D5TB02475G

neural cell culture purposes[4-7]. However, its effective and safe integration into 3D matrices remains poorly understood. This study aimed to assess PLL hydrogel biofunctionalization strategies that support neural cell adhesion, viability, differentiation, and maturation while preserving structural stability of the hydrogel matrix.

PLL is a well-established binding molecule that improves laminin retention and presentation in vitro[3], and can directly support cell adhesion through electrostatic interactions with cell membranes.[2] Its use has expanded to 3D hydrogel systems, but its effective translation from 2D to 3D environments remains challenging. Inconsistencies in reported PLL concentrations and molecular weights hinder reproducibility. Maintaining an optimal concentration of PLL is critical, as excessive levels induce cytotoxicity, disrupt cell morphology, and impair neural differentiation[8] , whereas insufficient concentrations may fail to promote cell adhesion or effective ECM adsorption. Moreover, the high net charge that provides PLL with its binding properties is also expected to impact on hydrogels swelling behaviour and compromise structural fidelity. Previous studies with other highly charged molecules, including heparin[9] and taurine[10] , have shown that electrostatic interactions can markedly alter PVA hydrogel formation, increasing equilibrium swelling by as much as five-fold and decreasing polymerization yield, reflected by mass losses approaching 50%. These findings highlight the need for strategies that preserve PLL bioactivity while maintaining structural control.

The main approaches for incorporating PLL into 3D matrices include chemical[6, 7] , and physical[4, 5] crosslinking, each presenting distinct advantages and limitations. Chemical crosslinking enables controlled, covalent integration of the biomolecule into the hydrogel matrix[11], typically through introduction of reactive groups like methacrylates[12]. Although methacrylation of PLL variants has been reported[13, 14], this strategy may interfere with the hydrogel crosslinking sites[9] and compromise bioactivity. For example, methacrylation can alter protein conformation and orientation[15], reducing cell attachment and proliferation[16, 17]. In contrast, physical blending of unmodified PLL provides a simpler alternative that avoids chemical modification while still potentially enhancing ECM retention and neural adhesion.[18] However, physical incorporation often yields less predictable distribution and weaker network integration.[11] Thus, achieving effective PLL incorporation remains challenging, as chemical modifications must balance structural stability with bioactivity.

View Article Online
DOI: 10.1039/D5TB02475G

The effectiveness of different PLL integration strategies should ultimately be evaluated by their ability to support functional neuronal development. This is commonly assessed through the expression of neuronal lineage markers and electrophysiological activity[19-21]. However, the formation of higher-order, functionally relevant neuronal structures, such as cell clusters and neural networks, has received less attention. Neuronal networks formed by interconnected neurons reproduce the complexity and dynamic signalling of in vivo circuitry[22], while neuronal clusters, defined as aggregated functional units, are known to enhance network activity[23]. Evaluating the emergence of these multicellular structures provides a more comprehensive measure of hydrogel performance for neural tissue modelling.

To address these gaps, this study developed a PVA-MA-based hydrogel (PVA-MA hydrogel) system incorporating PLL via two strategies: physical entanglement (blended PVA–PLL) and covalent conjugation (covalent PVA–PLL). PVA was selected for its structural stability, tuneable mechanics, and compatibility with methacrylate crosslinking[24, 25]. PLL concentration was systematically optimized to identify the minimal effective dose that retains laminin, supports motor neuron progenitors (MNPs) adhesion, and enables differentiation without inducing cytotoxicity or compromising hydrogel integrity. Finally, a morphometric analysis was applied to quantitatively assess the formation of clusters and networks, providing a more comprehensive evaluation of hydrogel performance for in vitro neural tissue modelling. Together, this work provides design criteria for integrating PLL into hydrogel biomaterials to support motor neuron culture and 3D network architectures.

2. Materials and methods

2.1. Methacrylation of PLL (PLL-MA) and PVA (PVA-MA)

Poly-L-lysine (PLL, 30–70 kDa; Sigma-Aldrich, P2636) was methacrylated following a protocol established for PVA modification[10] to enable its covalent integration into methacrylated hydrogel networks. Briefly, 500 mg of PLL was dissolved in 5 mL of dry DMSO at 60°C under a nitrogen atmosphere. Upon complete dissolution, 10.3 µL of 2-isocyanatoethyl methacrylate (ICEMA; Sigma-Aldrich, 98%) was added, targeting approximately 2% functionalization. For PVA-MA synthesis, 1 g of PVA (13–23 kDa, 98% hydrolyzed; Sigma-Aldrich, #348406) was dissolved in 10 mL of dry DMSO at 60°C under a nitrogen atmosphere. Then, 66.4 µL of ICEMA was added to achieve a theoretical substitution of ~7 methacrylate groups per PVA chain.

View Article Online
DOI: 10.1039/D5TB02475G

Following the reaction, both PLL-MA and PVA-MA were dissolved in deionized water (1 wt%) and transferred to 10 kDa molecular weight cutoff cellulose membranes (Sigma-Aldrich, D9402) for 5-day dialysis to remove unreacted reagents. The purified products were subsequently frozen and lyophilized. Methacrylation and the degree of functionalization were confirmed by ^{1}H NMR spectroscopy.

2.2. Cytocompatibility test of PLL-MA and PLL

Cytocompatibility of PLL-MA and PLL was assessed in accordance with the International Standard ISO 10993-5 via cell growth inhibition assays. Due to the higher sensitivity of MNP-D8 cells, L929 murine fibroblasts (Sigma Aldrich, USA) were used as a pre-screening indicator to identify non-toxic PLL concentrations suitable for neural applications. In the present study, a membrane integrity-based exclusion assay (trypan blue) was selected to directly assess material-associated cytotoxicity as a validated approach for assessing cytotoxic effects according to ISO 10993-5 guidelines. This approach enables detection of loss of plasma membrane integrity, a hallmark of acute cytotoxic response, and is widely used for initial screening of biomaterials. In brief, L929 cells were cultured in proliferation media consisting of Eagle's minimum essential media (Merck) supplemented with 10% FBS and 1% penicillin/streptomycin (P/S, Gibco) at 37°C in a 5% CO_2 atmosphere and passaged at 10×10^3 cells/cm² (passages 12-30).

Cell growth inhibition studies involved seeding 2 mL of L929 cells at 5×10^4 cells/mL in 35 mm dishes and culture for 24 h. Media was discarded and replaced with 1 mL of test solutions and incubated for an additional 48 h. Test solutions consisted of PLL and PLL-MA diluted to working concentrations of 0.2, 0.02, and 0.002 wt % in culture media. PVA-MA, as the main component of the hydrogel matrix, was included as a test solution which involved dissolving the macromolecular monomer (macromer) of PVA-MA at 1 wt % in PBS. Final dilutions maintained a 3:1 cell culture media to PBS ratio. Negative control (Nulls) consisted of cells in proliferation media only. Positive controls of toxicity involved exposing cells to 100% absolute ethanol diluted at 4%, 5%, and 7.5% v/v. After incubation, cells were rinsed twice with PBS and dissociated via 5 min incubation with 1 mL of TrypLE, then 500 µL of the cell suspension from each dish was collected and analysed using a cell viability analyser (Vi-cell XR, Beckman Coulter). Cell viability was calculated as described in Equation 1:

$$\text{Cell viability \%} = \left(\frac{Viable\ cell\ count}{Total\ cell\ count}\right) \times 100\% \quad (1)$$

View Article Online
DOI: 10.1039/D5TB02475G

2.3. Stability testing of physical versus covalent integration of PLL into PVA-MA hydrogels

To compare the effects of physical versus covalent integration of PLL into PVA-MA hydrogels, three hydrogel formulations were prepared, shown in Figure 1. First, PVA-MA hydrogels without PLL were used as a control (Figure 1A). The second variant involved blending unmodified PLL with PVA-MA prior polymerisation, where PLL was expected to physically crosslink with the PVA-MA network (Figure 1B). Finally, PVA-MA and PLL-MA were covalently crosslinked via photopolymerisation as described below (Figure 1C).

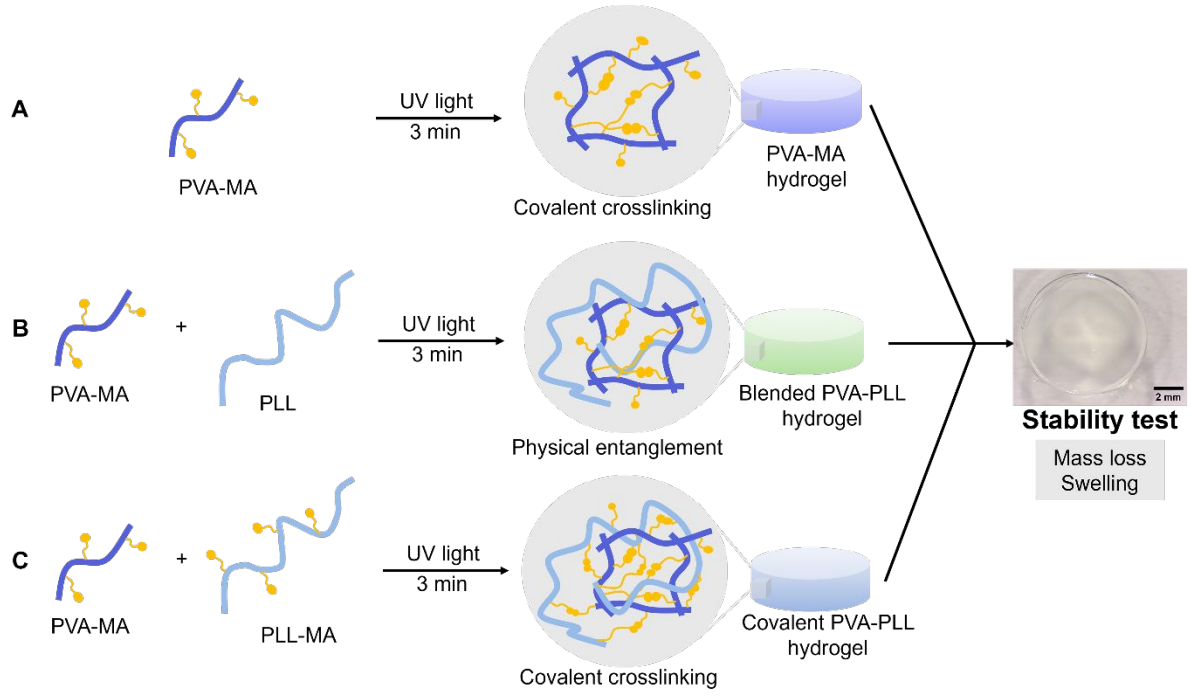

Figure 1. Schematic of PLL integration strategies into PVA-MA hydrogels for stability testing. (A) PVA-MA hydrogel (control), formed by covalent crosslinking of PVA-MA alone. (B) Blended PVA-PLL hydrogel, formed by physically mixing unmodified PLL with PVA-MA, resulting in physical entanglement of PLL within the network. (C) Covalent PVA-PLL hydrogel, formed by co-polymerising PVA-MA with methacrylated PLL (PLL-MA), enabling covalent incorporation of PLL into the network.

View Article Online
DOI: 10.1039/D5TB02475G

To fabricate hydrogels, PVA-MA macromers were dissolved at 15 wt% in PBS at 80°C. After cooling to room temperature, the photoinitiator 2-Hydroxy-4'-(2-hydroxyethoxy)-2-methylpropiophenone (Irgacure 2959) was added to reach a final concentration of 0.05 wt%. These hydrogels are not porous scaffolds, but rather homogeneous polymer networks formed via covalent crosslinking. For PLL-containing samples, a volume of 10 µL of PLL-MA or PLL solution was incorporated at a concentration informed by the cytotoxicity results, while PVA control hydrogels received an equivalent volume of PBS. Hydrogel precursor solutions were cast into silicone moulds (8 mm diameter, 0.5 mm thickness), and crosslinked under UV irradiation (BlueWave® 200, Dymax, 320-395 nm) at 30 mW/cm² for 3 minutes.

To evaluate the stability of PLL-integrated PVA hydrogels, mass loss and swelling assays were conducted following established protocols[26] that involved incubating hydrogels in PBS solutions at 37 °C for 1, 3 or 7 days. Mass loss was used to assess the amount of non-polymerized material leaching from the hydrogel matrix after curing, providing insights into polymerization efficiency. The volumetric swelling ratio measured the water absorption capacity of the hydrogel under swelling equilibrium conditions, reflecting its structural integrity and hydrophilicity.

In brief, all hydrogel samples were weighed directly after polymerization to establish the initial wet mass ($m_{initial,\,t0}$). Three samples were immediately lyophilized to obtain the initial dry weight ($m_{dry,\,t0}$), which is used to estimate the initial dry weights of the rest of the samples at t=0. This involves calculating the actual macromer fraction ($Act\text{-}Mac$ %) shown in Equation 2. The $Act\text{-}Mac$ % and $m_{initial,\,t0}$ were then used to calculate the initial dry weight of each sample (mi,dry) as shown in Equation 3.

$$Act\text{-}Mac\ \% = \frac{m_{dry,t_0}}{m_{initial,t_0}} \times 100\% \quad (2)$$

$$\mathrm{m_{i,dry}} = m_{initial,t0} \times Act\text{-}Mac\ \% \quad (3)$$

For each incubation time point, three hydrogel samples were removed from the incubator, blotted dry and weighed (m_{swollen}). The swollen samples were then lyophilized and weighed again (m_{dry}). The mass loss and volumetric swelling ratio were calculated as described in Equation 4 and 5, respectively.

$$Mass\ loss\ \% = \left(\frac{m_{i,dry} - m_{dry}}{m_{i,dry}}\right) \times 100\% \quad (4)$$

$$Volumetric\ swelling\ ratio = 1 + {\rho_{PVA}}/{\rho_{PBS}}\left(\frac{m_{swollen}}{m_{dry}} - 1\right) \quad (5)$$

View Article Online
DOI: 10.1039/D5TB02475G

2.4. Differentiation of human motor neuron progenitors

Motor neurons were differentiated from hESCs-H9 by adapting established protocols[19] described in detail in the supplementary material. In brief, as illustrated in Figure 2, the cell culture protocol involved proliferating human embryonic stem cells (hESCs-H9, WiCell), while inducing neural lineage followed by motor neuron specification. This protocol resulted in MNP spheroids over a period of 8 days on plastic petri dishes, referred to as MNP-D8. From Day 8 onward, cultures were supplemented with neurotrophic factors to promote neuronal differentiation and maturation. The key change to the cell culture protocol from Guo et al. [19], involved systematic evaluation of cell seeding density following spheroid dissociation.

MNP-D8 spheroids were dissociated using Accutase (Gibco A1110501), centrifuged at 300g for 3 minutes, and seeded at 7.5×10^4 cells/cm² on coverslips or hydrogel discs. The coverslips were pre-coated with PLL (Sigma, P5899, 100 µg/mL) and laminin (Gibco™ 23017015, 20 µg/mL). Differentiation progressed through defined stages. Motor neuron differentiation takes place on days 8-13 by supplementing medium with 0.1 µM retinoic acid (RA, Sigma R2625), 500 nM smoothened agonist (SAG, Sigma SML1314), 10 ng/mL brain derived neurotrophic factor (BDNF, Sigma B3795), 10 ng/mL glial derived neurotrophic factor (GDNF, Sigma G1777), and 10 µM of Inhibitor of γ-secretase (DAPT, Chem-Supply, GK0567). On Days 13-15 post-mitotic differentiation was induced with BDNF, GDNF, and increased DAPT (20 µM). In Days 15-29 culture medium consisted of BDNF, GDNF, and 10 ng/mL ciliary neurotrophic factor (CNTF, Sigma C3710) to promote neuronal maturation. According to the established protocol, this differentiation timeline yields motor neurons exhibiting morphological and molecular characteristics of mature motor neurons within approximately one month of differentiation. See supplementary materials for expanded details on cell maintenance, proliferation, and differentiation.

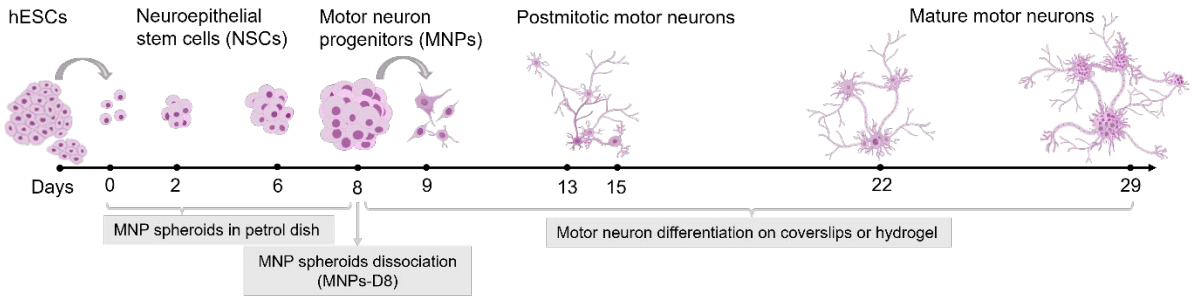

View Article Online
DOI: 10.1039/D5TB02475G

Figure 2. Illustration of the cell culture timeline for differentiating hESCs-H9 into motor neurons. MNP spheroids derived from hESCs-H9 were cultured in petri dishes for 8 days and dissociated on day 8 (MNPs-D8). Single cells MNPs-D8 were then plated on coverslips or hydrogels to induce motor neuron differentiation and neurite outgrowth. Image adapted from Guo et al.[19].

2.5. Presenting laminin to motor neurons via PLL-integrated PVA-MA hydrogels

The potential of PLL-integrated PVA-MA hydrogels to present laminin was assessed by growing MNP-D8 on PVA-MA, blended PVA-PLL, and covalent PVA-PLL hydrogels with or without laminin coating, as illustrated in Figure 3. First, PVA-MA, and both PVA-PLL hydrogels were steam sterilised (121 °C, 15 mins) while submerged in PBS. Hydrogels were transferred into a 24-well plate, and the excess of PBS was removed. A group of gels received a volume 50 µL of PBS containing 20 µg/mL of laminin, followed by an incubation at 37°C for 30 minutes. Coverslips pre-coated with PLL (100 µg/mL) and laminin (20 µg/mL) were used as control. MNPs adhesion, viability, and differentiation were assessed after 1, 3, and 7 days of culture on these substrates as described in Sections 2.6 and 2.7. MNP-D8 cells were seeded onto the hydrogels, resulting in a surface-based culture configuration. Two sets of hydrogel groups seeded with MNP-D8 were produced, one set was used for assessing cellular viability, and the second set to assess neuronal differentiation and morphometric analysis, both at 1, 3, and 7 days, corresponding to day 9, day 11, and day 15 of the differentiation timeline.

View Article Online
DOI: 10.1039/D5TB02475G

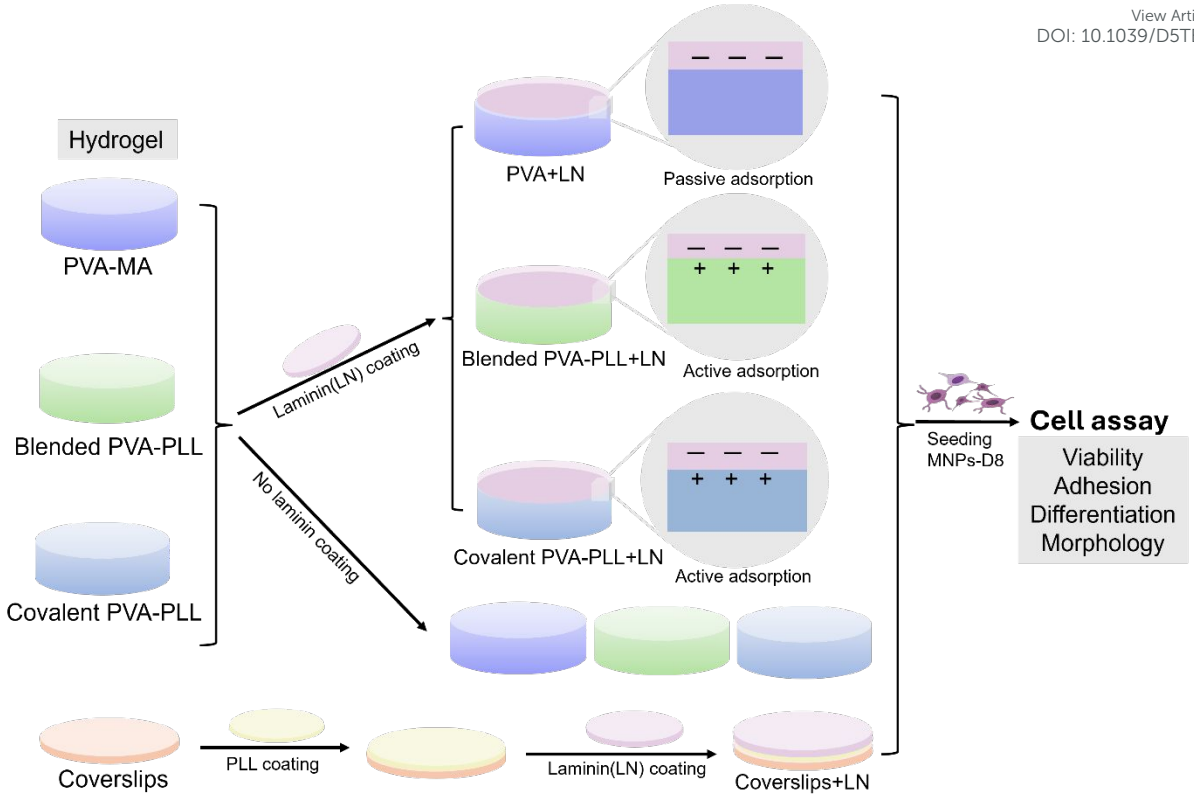

Figure 3. Experimental setup to evaluate laminin presentation on PLL-integrated PVA hydrogels. PVA, blended PVA-PLL, and covalent PVA-PLL were used to assess surface-mediated laminin binding and compared with a set without laminin coating. Electrostatic interactions in blended and covalent PVA-PLL hydrogels were expected to enhance laminin retention, while PVA relies on passive adsorption. Coverslips pre-coated with PLL and laminin served as positive controls. Motor neuron progenitors (MNP-D8) were seeded onto the substrates and cultured for 7 days and assessed for adhesion, viability, neuronal differentiation, and morphometric analysis.

2.6. Cell viability and adhesion on hydrogel substrates

The effects of PLL and PLL-MA integration on motor neuron progenitor (MNP-D8) viability and adhesion were assessed using live/dead staining and cell area coverage analysis. The experimental setup was illustrated on Figure 3. Cell viability was evaluated using a Calcein-AM/propidium iodide (PI) live/dead assay. Samples were incubated with 1 µM Calcein-AM and 1 µg/mL PI for 10 minutes, rinsed with PBS, and imaged using confocal microscopy. Live and dead cells were identified by green and red fluorescence, respectively. Using ImageJ software, viability was quantified as the ratio of the area covered by livings cells to that of

View Article Online
DOI: 10.1039/D5TB02475G

total cells, and cell attachment was measured as the percentage of cell-covered area relative to total image area by using ImageJ (National Institutes of Health, USA). For each sample, five fields were imaged, one at the centre and one in each of the four quadrants, to ensure unbiased spatial representation.

2.7. Assessment of neuronal differentiation and maturation

Differentiation was evaluated by immunostaining for key lineage markers supplemented with morphometric assessment of the formation of neuronal clusters and networks. The experimental setup was illustrated on Figure 3. Cells were fixed with 4% formaldehyde for 20 minutes, permeabilized using 0.1% Triton X-100 for 30 minutes and blocked with 2% bovine serum albumin (BSA) to minimize non-specific binding. Primary antibodies used included βIII-Tubulin (TUJ1, Abcam, #ab78078, 1:1000), oligodendrocyte transcription factor 2 (Olig2, Abcam, #ab109186, 1:200), Homeobox gene HB9 (HB9, Invitrogen, # PA5-23407, 1:1000), and Microtubule-associated protein 2 (MAP2, Abcam, #ab32454, 1:1000). After 1 hour at room temperature, samples were washed and incubated with Alexa Fluor 488 (Thermo Fisher, #A11008, 1:1000) and Alexa Fluor 594 (Thermo Fisher, #A11012, 1:1000) conjugated secondary antibodies for 1 hour at room temperature. TUJ1 was used for revealing neurites. HB9 and Olig2 are nuclei markers used to identify motor neuron lineage and progenitor status. MAP2 was used a marker of neuronal maturation. Nuclei were counterstained with 4',6-Diamidino-2-phenylindole dihydrochloride (DAPI, sigma-Aldrich). Samples were imaged by confocal microscopy to assess marker expression and neuronal morphology.

To assess the potential of PLL-integrated hydrogels in supporting motor neuron clustering and early network formation, a quantitative analysis was conducted by a blinded, independent assessor, who evaluated images of immunostained cells based on the questionnaire described in Table 1. This questionnaire, was designed to standardize assessment in cluster morphology, allowing for comparison of clustering behaviours and neurite organization across different substrates. The images consisted of MNP-D8 progressed to Day 15 of the differentiation process (Figure 2), here on referred to as day 7 of motor neuron differentiation on hydrogel. Day 7 was selected as a representative time point for evaluating early-stage cluster formation and neurite outgrowth. Samples included motor neurons cultured on three substrates: laminin-coated blended PVA-PLL (blended PVA-PLL+LN), laminin-coated covalent PVA-PLL

View Article Online
DOI: 10.1039/D5TB02475G

(covalent PVA-PLL+LN), and coverslips controls (coverslips+LN), each assessed with HB9/TUJ1 and Olig2/TUJ1 markers. Experiments were independently repeated three times (n=3), each with three replicates (N=9). Five fields per sample were acquired randomly, resulting in 90 images in total (45x HB9/TUJ1, and 45x Olig2/TUJ1). Image identifiers were removed, randomly numbered (1-90), and evaluated without knowledge of experimental groups.

Neuron aggregates were regarded a "cluster" if they met the following criteria: (1) ≥10 neuron cell bodies; (2) aggregation around a common centre; and (3) radial neurite outgrowth. Aggregates meeting two criteria were considered questionable clusters.

Table 1 Evaluation criteria for each cluster analysis

No.	Evaluation criteria	Answer Options
1	Are there any clusters present?	Yes, continue No
2	How many clusters are present in this image?	Numerical count
3	Is there a questionable cluster?	Yes No, continue
4	Shape of the cluster	Spherical Non-spherical
5	Cluster size (S)	Small (S ≤ 50 μm) Medium (50 μm < S < 100 μm) Large (S ≥ 100 μm)
6	Cell number (N) within the cluster	Low (N ≤ 15) Medium (15 < N < 40) High (N ≥ 40)
7	Distance (D) between clusters (measured from cluster centres)	Close (D ≤ 50 μm) Medium (50 μm < D < 100 μm) Far (D ≥ 100 μm)

2.9. Statistical analysis

All values are presented as the mean of three independent experiments (n = 3), each with three technical replicates (N = 9). Data normality was assessed using Quantile-Quantile (Q-Q) plots prior to statistical analysis. Parametric tests were applied when data exhibited approximately normal distribution. Depending on the number of factors or predictors, either one-way or two-way ANOVA was performed to determine statistical differences, followed by Tukey-Kramer post hoc tests for multiple comparisons. Results were reported as mean ± standard deviation (SD). Statistical significance was defined at $p < 0.05$, with significance levels

View Article Online
DOI: 10.1039/D5TB02475G

indicated as *0.01< p < 0.05, **p < 0.01, ***p < 0.001, and ****p < 0.0001. All analyses were performed using GraphPad Prism version 10.2.0.

3. Results

3.1. Characterization and cytocompatibility of PLL and PLL-MA

As shown in Figure 4A, the ^{1}H NMR spectrum of unmodified PLL displayed characteristic peaks corresponding to the native PLL backbone. In contrast, the spectrum of PLL-MA (Figure 4B) exhibited additional vinyl proton signals at 6.1 and 5.7 ppm, along with new resonances in the 3.1-3.5 ppm region. These spectral changes confirmed the successful introduction of methacrylate groups, providing reactive sites for covalent crosslinking in hydrogel networks.

Cytocompatibility analysis (Figure 4C-D) revealed that both PLL and PLL-MA were markedly cytotoxic at 0.02 wt% and 0.2 wt%, reducing cellular viability to below 20% and causing severe morphological damage characterized by extensive cell debris. Toxicity at these concentrations exceeded that of the 7.5% ethanol positive control. At 0.002 wt%, unmodified PLL remained moderately cytotoxic, yielding ~55% viable cells with evident debris and irregular, star-shaped morphologies, contrasting to the confluent spindle-shaped fibroblasts observed in the negative controls (95-100% viability). In comparison, PLL-MA at 0.002 wt% maintained ~87% viability, with only slight inhibition of cell proliferation and fewer morphological abnormalities. As anticipated, PVA-MA exhibited negligible cytotoxicity comparable to the blank controls, whereas ethanol-treated positive controls confirmed assay validity. Based on minimal toxicity and acceptable compatibility, 0.002 wt% PLL-MA was selected for subsequent hydrogel integration studies. Because the extent of PLL incorporation within the hydrogel matrix was uncertain, unmodified PLL at 0.002 wt% was also examined to account for the potential influence of non-incorporated polymer.

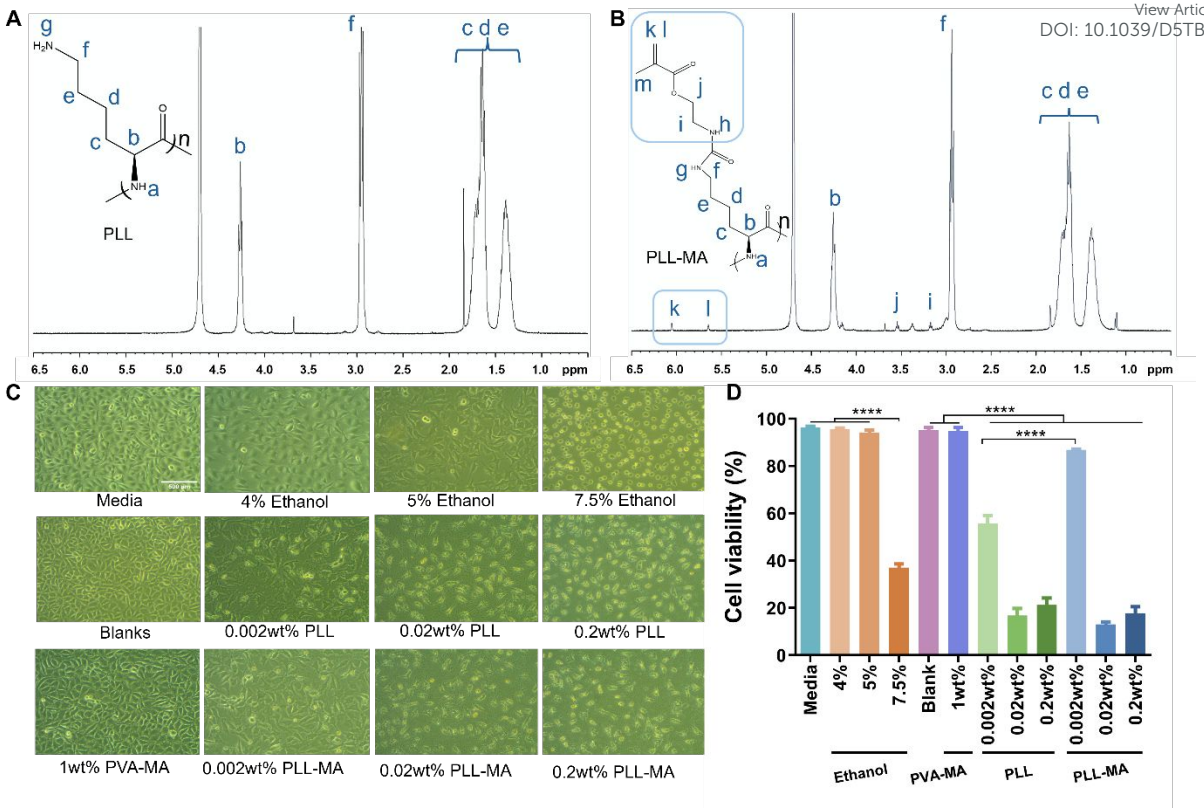

Figure 4. Characterization of PLL-MA polymer synthesis and cytocompatibility of PLL and PLL-MA polymer. ^{1}H NMR spectra of PLL (A) and PLL-MA (B) in D_2O, showing characteristic proton signals for structural confirmation of unmodified PLL and methacrylated PLL. (C) Representative phase-contrast images of L929 cells after 2-day culture with PVA-MA, PLL, or PLL-MA polymer treatments, highlighting morphological differences associated with polymer exposure. (D) Quantitative analysis of cell viability after a 2-day culture period with PVA-MA, PLL, and PLL-MA polymers.

3.2. Stability of PLL-integrated hydrogels

On day 1, the mass loss of covalently crosslinked PVA-PLL hydrogels was comparable to that of PVA-MA controls (Figure 5A). Covalent PVA-PLL exhibited a slightly lower mass loss than blended PVA-PLL, which showed approximately threefold greater mass loss relative to PVA-MA gels. Over time, however, the mass loss of all hydrogel formulations plateaued and remained below 10%. These findings suggest that the amount of unreacted or soluble polymer is minimal and largely independent of PLL incorporation, although the presence of PLL may enhance the leaching rate of non-crosslinked polymer fractions.

View Article Online
DOI: 10.1039/D5TB02475G

Swelling analysis revealed that all hydrogel formulations reached a peak swelling ratio of approximately six on day 1, with no statistically significant differences observed among groups over the 7-day period (Figure 5B). Thus, the incorporation of PLL or PLL-MA did not notably alter the equilibrium water uptake of hydrogels. Altogether, swelling behaviour and mass loss suggest that effective network crosslinking stabilizes within the first few days. These findings confirmed that PLL and PLL-MA incorporation maintains hydrogel stability.

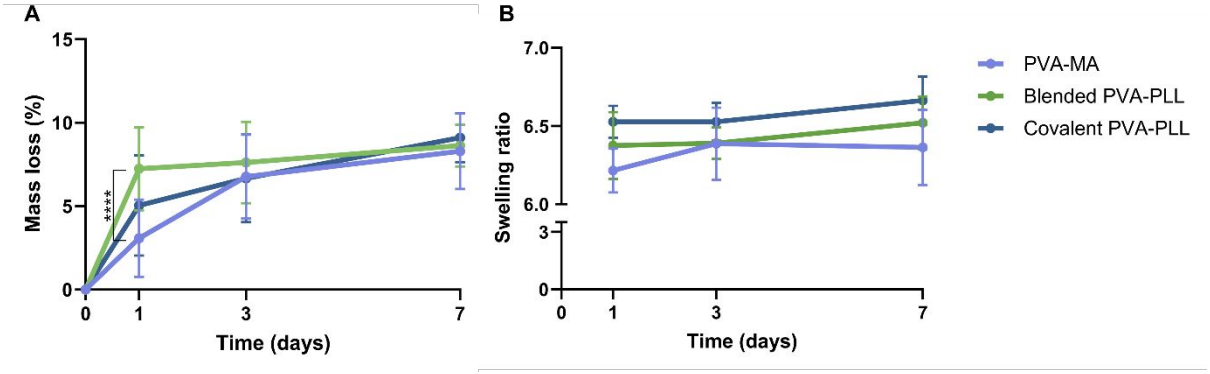

Figure 5. Stability assessment of PLL-integrated hydrogels. Mass loss (A) and swelling ratio (B) analysis of 15 wt% PVA-MA, blended PVA-PLL, and covalent PVA-PLL hydrogels over a 7-day period.

3.3. Presenting Laminin for promoting motor neuron viability and attachment via PLL-integrated PVA hydrogels

Phase-contrast images (Figure 6A, Figure S1) showed morphological changes throughout hESC-H9 derived motor neuron differentiation process. hESCs-H9 were efficiently directed toward a motor neuron lineage, as evidenced by robust Olig2 expression on day 9, indicative of early motor neuron progenitor specification (Figure 6B). As differentiation progressed, Olig2 expression markedly declined, coinciding with the emergence of MAP2-positive neurons, confirming neuronal maturation (Figure 6B, Figure S2). Persistent HB9 expression throughout differentiation verified motor neuron lineage commitment, while TUJ1 immunostaining demonstrated extensive neurite outgrowth characteristic of functional neuronal morphology (Figure 6B). The results of morphological progression and marker expression presented the validation of the motor neuron differentiation protocol on PLL and Laminin coated coverslip (Coverslips+LN) controls. Overall, adjustment of cell seeding density in the differentiation

View Article Online
DOI: 10.1039/D5TB02475G

protocol resulted in human motor neuron cultures enriched in neuronal clusters and interconnected networks, thereby improving upon existing differentiation protocols.

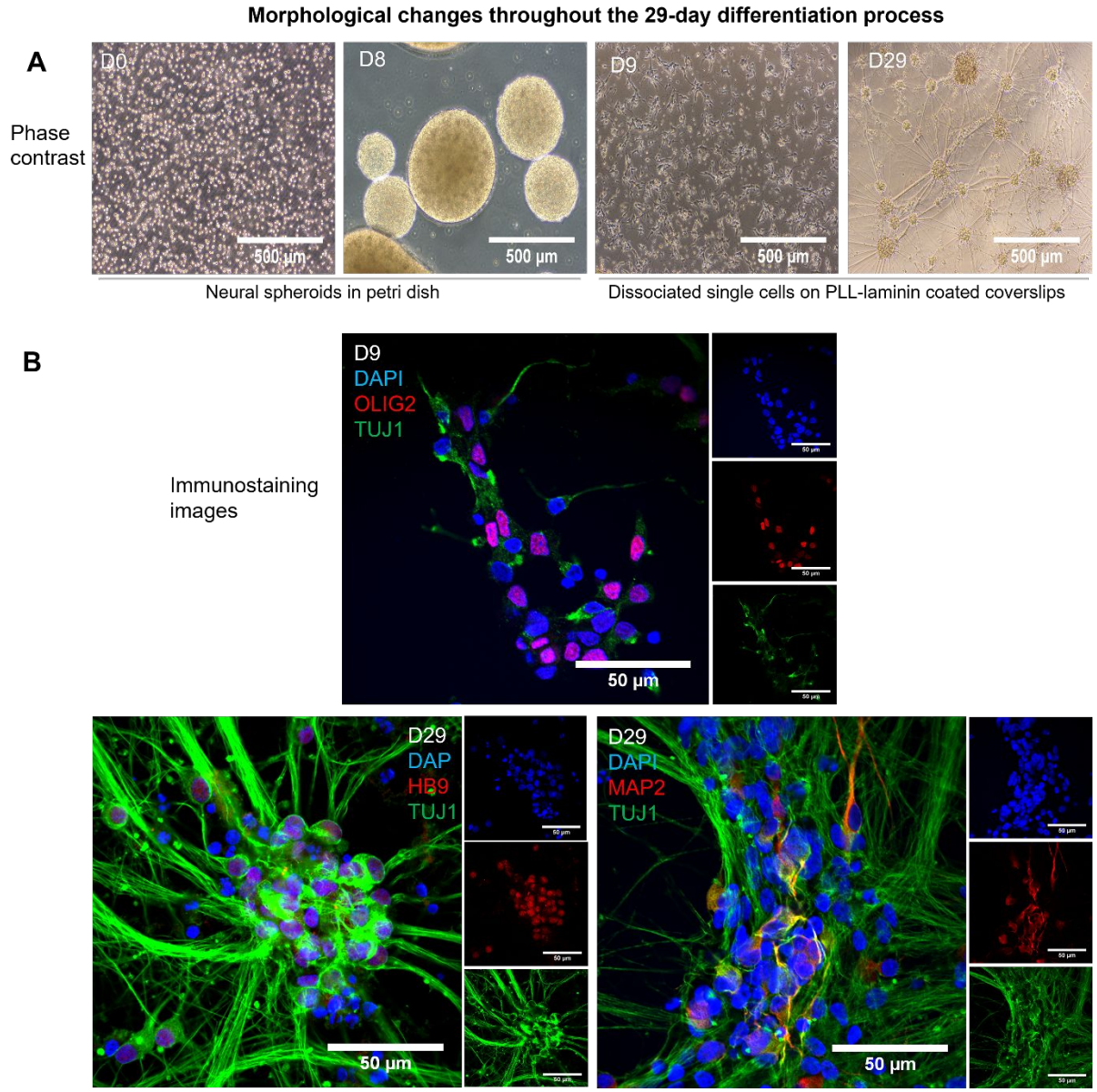

Figure 6. **Morphological progression and marker expression during hESC-H9-derived motor neuron differentiation.** (A) Phase-contrast images showing morphological changes throughout the differentiation process from petri dish (D0 and D8) and PLL-Laminin coated coverslips (D9 and D29). Scale bars = 500 µm. (B) Representative immunostaining images at D9and D29 on coverslips highlighting sequential expression of motor neuron markers. TUJ1 (green) labels neuronal axons, Olig2 (red) marks motor neuron progenitors, HB9 (red)

View Article Online
DOI: 10.1039/D5TB02475G

identifies post-mitotic motor neurons, MAP2 (red) indicates mature dendritic structures, and DAPI (blue) stains nuclei. Scale bars = 50 µm.

When MNP-D8 cells were cultured on hydrogel substrates, overall viability was comparable to Coverslips+LN controls, suggesting that neither physical nor chemical integration of PLL adversely affected cell viability. Cell growth and adhesion varied depending on the PLL incorporation strategy, and the presence of laminin coatings (Figure 7). As expected, unmodified PVA-MA hydrogels exhibited negligible cell adhesion, confirming their lack of inherent bioactivity (Figure 7A-C). In contrast, both blended and covalently linked PVA-PLL hydrogels supported robust cell attachment even in the absence of laminin (Figure 7A-C). Laminin coating further promoted neurite extension and cell spreading, with minimal detachment observed on blended PVA-PLL+LN and covalent PVA-PLL+LN compared to PVA alone (Figure 7A-C). Notably, the performance of covalent PVA-PLL+LN was comparable to standard PLL-Laminin coated coverslips (Figure 7A-C).

Quantification confirmed these observations. Cell viability remained consistently high (65-85%) across all PLL and PLL-MA integrated hydrogels, irrespective of laminin coating (Figure 7D-F). On Day 1, cell area coverage was low on all hydrogel variants (5-10%), below that of coverslip controls (~15%) (Figure 7G). By Day 3, adhesion on blended PVA-PLL remained limited (~10%), similar to PVA+LN, but increased to ~20% with laminin coating (Figure 7H). At this time point, covalent PVA-PLL, with or without laminin, supported significantly greater adhesion, comparable to coverslip controls (~25%). By Day 7, clear trends emerged. Laminin coating enhanced cell area coverage more than threefold in blended PVA-PLL+LN hydrogels (36.3%) relative to uncoated counterparts, comparable to the increase observed in PVA-MA+LN gels (Figure 7I). In covalent PVA-PLL variants, laminin similarly promoted coverage (42.2%), representing a 1.6-fold increase over uncoated PVA-PLL, with no significant difference compared to laminin-coated coverslip controls (49.1%) (Figure 7I). The large variability in the PVA-MA+LN gels was attributed to heterogeneous laminin retention. Many gels failed to retain laminin and supported no cell adhesions, whereas, in others laminin may have been retained via weak adsorption to PVA-MA chains.

Collectively, these data demonstrated that PLL-MA integration markedly enhanced hydrogel biofunctionality by improving laminin retention and sustaining motor neuron progenitor

View Article Online
DOI: 10.1039/D5TB02475G

viability, adhesion, and differentiation at levels comparable to conventional gold standard techniques.

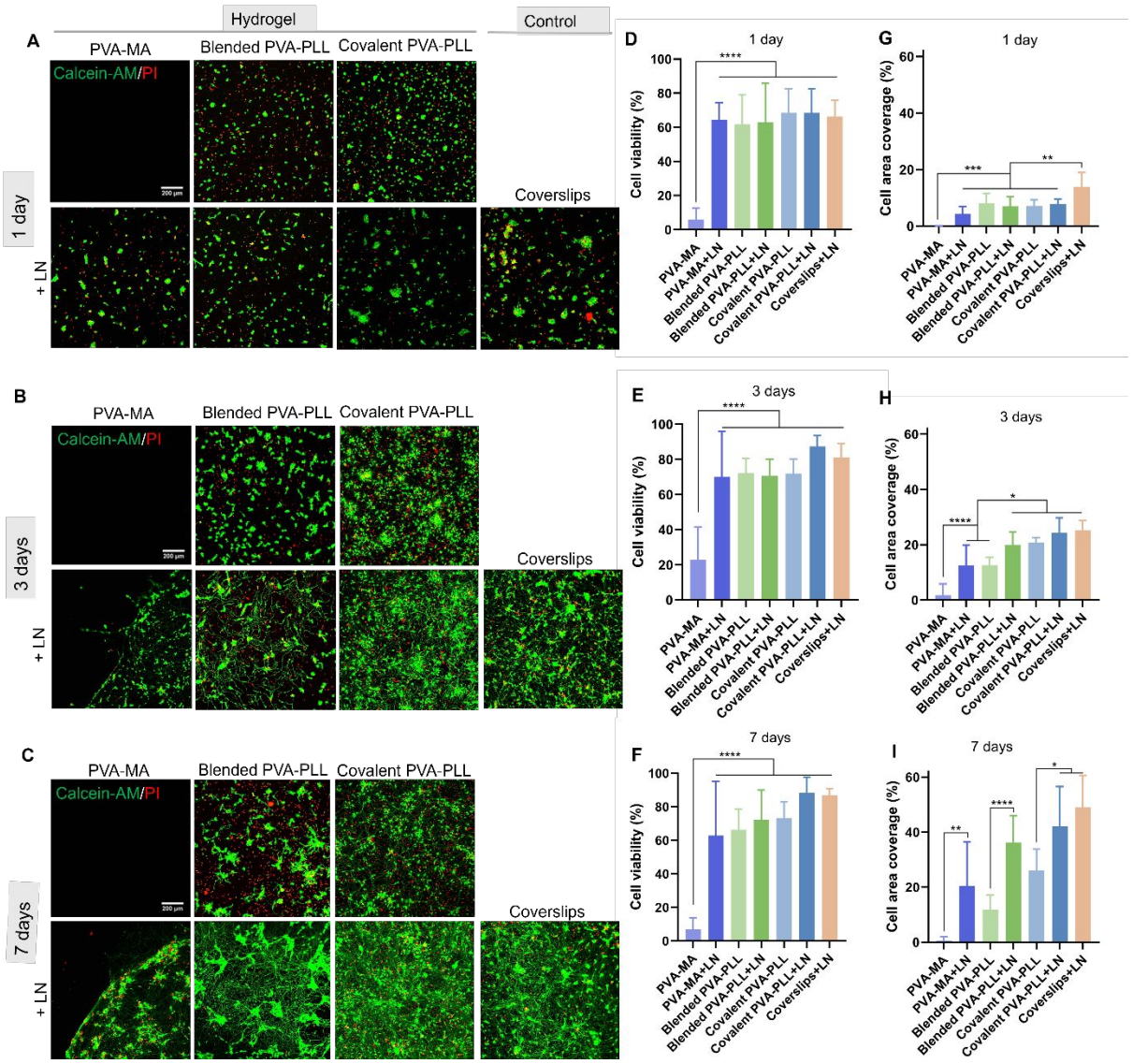

Figure 7. Viability and adhesion of motor neuron progenitors (MNP-D8) on PLL-integrated PVA hydrogels. Representative live/dead staining images of MNP-D8 on day 1 (A), day 3 (B), and day 7 (C) across different substrates. Live cells are stained with Calcein-AM (green) and dead cells with propidium iodide (PI, red); scale bar = 200 µm. (D-F) Quantification of cell viability (%) at days 1, 3, and 7, respectively. (G-I) Quantification of cell area coverage (%) at days 1, 3, and 7, respectively.

View Article Online
DOI: 10.1039/D5TB02475G

3.4. Promoting motor neuron differentiation via PLL-integrated PVA hydrogel presenting laminin

On day 1, all groups exhibited initial adhesion (Figure 8A), characterized by limited neurite outgrowth and co-expression of early neuronal markers TUJ1 and HB9 together with Olig2, indicating the presence of undifferentiated progenitors. By day 3, neurite extension became more pronounced, Olig2 expression slightly decreased in intensity, and HB9/TUJ1 signals intensified, reflecting early neuronal differentiation and initiation of network formation (Figure 8B).

By day 7, both blended and covalent PVA-PLL+LN hydrogels promoted pronounced neuronal clustering, and more extensive neurite networks relative to coverslips (Figure 8C). Both hydrogels supported stronger HB9 and TUJ1 expression with diminished Olig2 levels, indicative of a shift toward more mature motor phenotypes (Figure 8A-C). Notably, covalent PVA-PLL+LN hydrogels yielded the most complex and interconnected networks, followed by the blended formulation, while coverslips exhibited limited clustering and sparse neurite projections.

Cluster analysis at day 7 revealed clear differences in motor neuron organization across blended PVA-PLL+LN, covalent PVA-PLL+LN hydrogels, and coverslips (Figure 8D-H). Both blended and covalent PVA-PLL+LN hydrogels exhibited high cluster presence rates (96.7% and 93.3%, respectively), whereas coverslips displayed significantly fewer clusters (50%), confirming enhanced cluster formation on hydrogel substrates (Figure 8D). Moreover, hydrogel-based cultures promoted more stable and uniform cluster morphology, with a higher proportion of spherical clusters (68.5% for blended PVA-PLL+LN and 74% for covalent PVA-PLL+LN), in contrast to coverslips which showed 46.4% spherical clusters (Figure 8E).

Although all hydrogel formulations supported clusters ranging from tens to over one hundred micrometres in diameter (Figure 8F), distinct differences in cluster density and inter-cluster spacing were observed (Figure 8G, H). Covalent PVA-PLL+LN hydrogels favoured the formation of large, high-density clusters (>40 cells per cluster, 43.3%), whereas blended PVA-PLL+LN primarily yielded low-density clusters (<15 cells, 54%) with moderate formation of intermediate (15-40 cells, 28%) and high-density clusters (~15%) (Figure 8G). Coverslip cultures predominantly exhibited small, low-density clusters (77.4%) (Figure 8G). Spatial

View Article Online
DOI: 10.1039/D5TB02475G

distribution analysis revealed further substrate-dependent organization (Figure 8H). Covalent PVA-PLL+LN hydrogels promoted closer cluster proximity (66.7% within 50 µm), while blended hydrogels exhibited a more balanced distance profile, and coverslips showed predominantly dispersed clusters (75% >100 µm) (Figure 8H).

Overall, PLL-integrated PVA hydrogels, particularly covalently crosslinked formulations, fostered the formation of denser, spatially coordinated, and highly interconnected neural clusters compared to traditional 2D substrates.

View Article Online
DOI: 10.1039/D5TB02475G

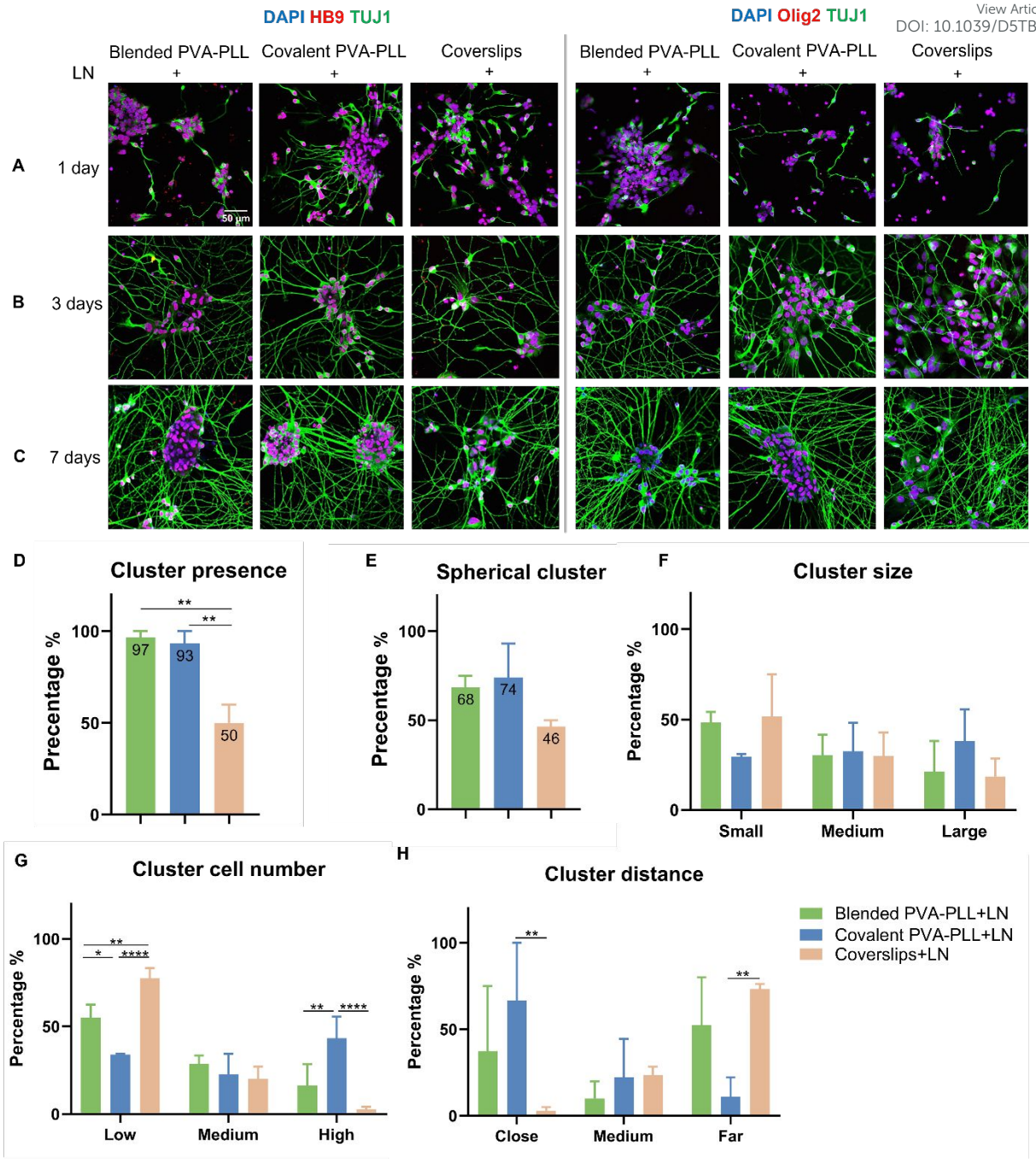

Figure 8. Motor neuron cluster formation and spatial organization across different laminin-presenting substrates. Representative immunofluorescence images of MNP-D8 on day 1 (A), day 3 (B) and day 7 (C) of differentiation, stained for TUJ1 (green), HB9 or Olig2 (red), and DAPI (blue), on blended PVA-PLL+LN, covalent PVA-PLL+LN, and coverslips+LN; scale bar = 50 µm. Quantitative analysis of cluster morphology at day 7, including: cluster presence rate (D), spherical cluster rate (E), cluster size distribution (F), cluster cell number (G), and inter-cluster distance (H).

View Article Online
DOI: 10.1039/D5TB02475G

4. Discussion

This study elucidated how incorporation strategies of PLL modulates the physicochemical stability of PVA-MA hydrogels and influences neural differentiation outcomes and network architectures. The concentration-dependent cytotoxicity of PLL stresses the need of its precise titration in 3D matrices. Among the tested formulations, only the lowest concentration (0.002 wt%) proved minimally toxic. At this concentration, PLL either blended or covalently crosslinked, preserved hydrogel network integrity while enhancing laminin retention and supporting MNPs differentiation comparable to conventional PLL-laminin coated coverslip substrates. These findings addressed a critical gap in the literature by defining the minimal effective PLL concentration required to sustain neuronal differentiation in hydrogel systems. Moreover, this work introduced an expanded analytical framework for evaluating neural differentiation by integrating classical molecular markers with quantitative assessments of cluster morphology and network connectivity. Overall, this study offered a more holistic understanding of neural maturation within engineered microenvironments.

PLL is widely recognized for improving cell adhesion by providing a positively charged surface that facilitates protein adsorption, particularly for ECM components such as laminin.[27] The strong electrostatic interactions between PLL and laminin creates a bioactive surface, which promotes neural progenitor attachment and differentiation.[3] While previous studies have examined the role of PLL in 2D and to an extent within hydrogel substrates[28], the effective incorporation into 3D hydrogel environments has remained insufficiently characterized. Earlier investigations used much higher PLL concentrations (>0.01 wt%) to coat culture surfaces or hydrogels[5, 6, 8], concentrations shown in the present study as cytotoxic. For example, Karimi-Soflou *et al.* cultured P19 embryonic stem cells on PLL/alginate/polypyrrole hydrogels containing 1 wt% PLL and reported heterogeneous cell viability. However, the presence of additional copolymer components and low crosslink density may have masked direct PLL toxicity. In contrast, these findings demonstrated that a significantly lower PLL concentration (0.002 wt%) was sufficient to improve cell adhesion and differentiation without compromising bioactivity.

Given the cationic nature of PLL, its inclusion can increase hydrogel swelling through charge-driven osmotic effects, potentially influencing mechanical stability and cell-matrix interaction[8]. While the influence of PLL on PVA hydrogels has not been studied, analogous

View Article Online
DOI: 10.1039/D5TB02475G

charged biomolecule incorporations are known to increase in mass loss above 25% and induced large volumetric swelling ratios in the range of tens to hundreds[29]. Analogue systems have reported volumetric swelling ratios in the 10-15 range when covalently crosslinking 10 wt% diacrylate poly(ethylene glycol) (PEG, 1.5 - 10 kDa) with PLL (70 - 150 kDa) [6, 8]. In these studies, the PLL concentration used was at least two orders of magnitude greater than the one used here. Of remark, the 0.002 wt% PLL maintained mass loss below 10% and swelling ratios around 6, values consistent with reported benchmarks for stable PVA-based systems[9, 10]. Of note, changes in hydrogel swelling behavior are directly related to variations in network crosslink density, which in turn governs mechanical propertiess[30]. As PLL incorporation did not significantly affect swelling, the crosslinked network structure of PVA-MA hydrogels is expected to remain unchanged. Consequently, the mechanical properties of PVA/PLL hydrogels are anticipated to be comparable to those of the base PVA-MA formulation. However, although PLL was incorporated at low concentration, covalent tethering increased compressive modulus by ~31% (see supplementary Section 3), suggesting localized network alterations. This effect was reversed by steam sterilization, while bioactivity remained intact, indicating preservation of PLL.

Covalent crosslinking of PLL-MA was hypothesized to further stabilize the network by restricting polymer mobility. However, mass-loss profiles were comparable between covalently crosslinked and physically blended systems, suggesting that at such low PLL content, the structural contribution is negligible. While Zhou et al.[18] and Karimi-Soflou et al.[5] reported markedly different swelling ratios for PLL-modified hydrogels based on hyaluronic acid and alginate/polypyrrole matrices, respectively, these variations largely reflect differences in polymer composition and formulation. Importantly, neither study systematically isolated the effect of PLL on hydrogel stability, limiting direct comparison with the present findings.

Laminin-coated PVA-PLL hydrogels effectively supported differentiation of MNP-D8 progenitors into mature motor neurons, achieving performance comparable to conventional PLL/laminin-coated coverslips[19]. This study shows for the first time the culture and differentiation of motor neurons on laminin coated PVA-PLL hydrogels. Analogue PEG-based hydrogels incorporating PLL have also been studied to support development of neural progenitor cells[6, 8], however these systems with cells expressing lineage markers, typically

View Article Online
DOI: 10.1039/D5TB02475G

exhibit minimal clustering and network formation. Differences in backbone chemistry, macromer content, and PLL dosage complicate direct comparison between PEG and PVA matrices. Nevertheless, the current findings indicate that PLL contributes primarily to local bioactivity by enhancing laminin retention and cell adhesion, without altering the bulk physicochemical properties of the hydrogel.

Collectively, these observations establish that finely tuned PLL incorporation preserves hydrogel structural integrity while enabling laminin-mediated signalling essential for neuronal differentiation. To assess whether these molecular optimizations translate into higher-order neural organization, this study next examined the spatial distribution and connectivity of differentiating cells within the hydrogels. Cluster analyses revealed enhanced neural organization in PLL-integrated hydrogels, characterized by increased cluster prevalence, and more mature network morphology relative to coverslip controls. Conventional motor neuron differentiation studies have primarily relied on single-cell morphology assessments, marker expression analysis, and neurite length measurements[20, 21] , which fail to capture the spatial complexity inherent to neural tissues. By incorporating blinded evaluations of cluster formation and network connectivity, this study provides a more unbiased and physiologically relevant representation of neuronal organization. In this context, neural clusters reflect early assemblies of differentiating neurons establishing functional contacts, while interconnected networks denote advanced maturation. Although the biological relevance of these structures in motor neuron systems remains to be fully elucidated, these insights collectively emphasize the importance of microenvironmental design in directing neural network formation and functional integration.

Despite these advances, the present study is limited to early differentiation stages and does not assess long-term neuronal functionality, such as synaptic transmission or electrophysiological maturation. Future work should therefore examine whether neurons cultured on PLL-functionalized PVA-MA hydrogels establish functional synapses and exhibit mature firing dynamics. Additionally, further optimization of hydrogel architecture, through modulation of stiffness, crosslinking density, or incorporation of complementary ECM components, may enable extended axonal outgrowth and more complex network topologies.

The ultimate application of this platform lies in the development of structurally defined in vitro neural tissue models. Hydrogels are widely recognized as biomaterials with tissue-

View Article Online
DOI: 10.1039/D5TB02475G

mimetic mechanical and physicochemical properties, making them attractive substrates for engineered constructs. A key consideration in hydrogel selection is the trade-off between biologically derived materials, which inherently support cell–matrix interactions, and synthetic systems, which offer greater control over mechanical properties and spatial presentation of bioactive cues. Synthetic hydrogels are therefore particularly advantageous for precisely tuning scaffold architecture and biomolecular functionalization.

For example, laminins play critical roles in synaptic maturation, axonal outgrowth, and neuronal stability[31], while collagens provide structural support and contribute to axonal guidance and neurotransmission[32] . The controlled and spatially defined presentation of such biomolecules is essential for generating in vitro neural models that more closely recapitulate native tissue organization.

Here, we demonstrate that PLL can be incorporated into PVA-MA hydrogels without compromising structural integrity. Importantly, PVA hydrogels can be fabricated into macroscale and tubular geometries[33] relevant to peripheral nerve guidance applications. Together, these properties position the PVA/PLL system as a scalable and adaptable platform for engineering organized neural tissue models, with potential applications in motor neuron biology, regenerative medicine, and in vitro disease modelling.

In summary, this work established that minimally dosed PLL integration into PVA-MA hydrogels yields a stable, biocompatible platform capable of supporting robust motor neuron differentiation and early network formation. The approach offers a scalable, physiologically relevant model system with potential applications in neural tissue engineering, disease modelling, and regenerative neurobiology.

5. Conclusions

This study demonstrated that tailoring PLL content and attachment within PVA-MA hydrogels enables the creation of stable and bioactive matrices that support motor neuron differentiation and early network formation. A minimal PLL concentration (0.002 wt%) was identified as optimal, preserving hydrogel integrity while enhancing laminin retention, cellular adhesion, and neural maturation. The integration of quantitative network and cluster analyses provided deeper insight into the spatial organization of differentiating neurons

within 3D environments, with evidence for physical and chemical conjugation approaches differentially guiding network architecture. Collectively, these findings establish a framework for the rational design of neural biomaterials in which minimal biofunctionalization achieves biological efficacy, advancing the development of physiologically relevant models for neural tissue engineering and regenerative neurobiology.

Author Contributions

Shuqian Wan: Conceptualization, project administration, formal analysis, methodology, writing - original draft, writing – review & editing, investigation.

Ulises Aregueta Robles: Conceptualization, resources, supervision, formal Analysis, methodology, writing – review & editing, Investigation

Laura Poole-Warren: Conceptualization, resources, supervision**,** formal Analysis, funding acquisition, writing – review & editing

Dorna Esrafilzadeh: Project administration, resources, supervision, funding acquisition, writing – review & editing

Kristopher A. Kilian: Resources, supervision, writing – review & editing

Conflicts of interest

The authors declare that they have no known competing financial interests or personal relationships that could have appeared to influence the work reported in this paper.

Acknowledgements

The authors gratefully acknowledge the support from UNSW Scientia fellowship support fund. We thank Prof. Penny Martens and Dr Rebecca Sehnert from Biosynthetic Hydrogels Group at School of Biomedical Engineering for technical assistance with polymer analysis. We are also thankful to David Chan from Stats Central, Mark Wainwright Analytical Centre at UNSW for his valuable statistical consultation.

Reference

1. S. Mohanty and S. Roy, *Macromol Biosci*, 2024, **24**, e2400207.
2. S. S. Rao and J. O. Winter, *Front Neuroeng*, 2009, **2**, 6.

3. D. Liu, N. Pavathuparambil Abdul Manaph, M. Al-Hawwas, L. Bobrovskaya, L.-L. Xiong and X.-F. Zhou, *Stem Cells and Development*, 2020, **29**, 463-474.
4. Y. Zhou, L. Kang, Z. Yue, X. Liu and G. G. Wallace, *ACS Applied Bio Materials*, 2020, **3**, 628-638.
5. R. Karimi-Soflou, I. Shabani and A. Karkhaneh, *International Journal of Biological Macromolecules*, 2023, **237**, 124063.
6. L. Cai, J. Lu, V. Sheen and S. Wang, *Biomacromolecules*, 2012, **13**, 1663-1674.
7. S. Royce Hynes, L. M. McGregor, M. Ford Rauch and E. B. Lavik, *Journal of Biomaterials Science, Polymer Edition*, 2007, **18**, 1017-1030.
8. S. R. Hynes, M. F. Rauch, J. P. Bertram and E. B. Lavik, *Journal of Biomedical Materials Research Part A*, 2009, **89A**, 499-509.
9. A. Nilasaroya, L. A. Poole-Warren, J. M. Whitelock and P. Jo Martens, *Biomaterials*, 2008, **29**, 4658-4664.
10. J. Goding, A. Gilmour, P. Martens, L. Poole-Warren and R. Green, *Adv Healthc Mater*, 2017, **6**.
11. Y. S. Zhang and A. Khademhosseini, *Science*, 2017, **356**, eaaf3627.
12. M. A. Daniele, A. A. Adams, J. Naciri, S. H. North and F. S. Ligler, *Biomaterials*, 2014, **35**, 1845-1856.
13. C. Zhou, P. Li, X. Qi, A. R. M. Sharif, Y. F. Poon, Y. Cao, M. W. Chang, S. S. J. Leong and M. B. Chan-Park, *Biomaterials*, 2011, **32**, 2704-2712.
14. Z. Meng, Y. He, F. Wang, R. Hang, X. Zhang, X. Huang and X. Yao, *ACS Applied Bio Materials*, 2021, **4**, 2713-2722.
15. S. Sen-Britain, W. L. Hicks, Jr., R. Hard and J. A. Gardella, Jr., *Biointerphases*, 2018, **13**, 06e406.
16. A. Joy, D. M. Cohen, A. Luk, E. Anim-Danso, C. Chen and J. Kohn, *Langmuir*, 2011, **27**, 1891-1899.
17. J. E. Samorezov, C. M. Morlock and E. Alsberg, *Bioconjugate Chemistry*, 2015, **26**, 1339-1347.
18. Y. Zhou, L. Kang, Z. Yue, X. Liu and G. G. Wallace, *ACS Applied Bio Materials*, 2020, **3**, 628-638.
19. W. Guo, M. Naujock, L. Fumagalli, T. Vandoorne, P. Baatsen, R. Boon, L. Ordovás, A. Patel, M. Welters, T. Vanwelden, N. Geens, T. Tricot, V. Benoy, J. Steyaert, C. Lefebvre-Omar, W. Boesmans, M. Jarpe, J. Sterneckert, F. Wegner, S. Petri, D. Bohl, P. Vanden Berghe, W. Robberecht, P. Van Damme, C. Verfaillie and L. Van Den Bosch, *Nat Commun*, 2017, **8**, 861.
20. B. S. Jha, M. Rao and N. Malik, *Stem Cell Rev Rep*, 2015, **11**, 194-204.
21. M. S. Fernandopulle, R. Prestil, C. Grunseich, C. Wang, L. Gan and M. E. Ward, *Current Protocols in Cell Biology*, 2018, **79**, e51.
22. T. B. Puschmann, Y. de Pablo, C. Zandén, J. Liu and M. Pekny, *Tissue Engineering Part C: Methods*, 2014, **20**, 485-492.
23. M. Shein Idelson, E. Ben-Jacob and Y. Hanein, *PLOS ONE*, 2011, **5**, e14443.
24. P. Martens, J. Blundo, A. Nilasaroya, R. A. Odell, J. Cooper-White and L. A. Poole-Warren, *Chemistry of Materials*, 2007, **19**, 2641-2648.
25. P. Martens and K. S. Anseth, *Polymer*, 2000, **41**, 7715-7722.
26. A. A. R. Ulises, *Journal of polymer science*, 2018, **v. 56**, pp. 273-287-2018 v.2056 no.2014.
27. X. Zhang, T. Viitala, R. Harjumäki, A. Kartal-Hodzic, J. J. Valle-Delgado and M. Österberg, *Journal of Colloid and Interface Science*, 2021, **584**, 310-319.

28. C. Wu, S. Liu, L. Zhou, Z. Chen, Q. Yang, Y. Cui, M. Chen, L. Li, B. Ke and C. Li, *ACS Applied Materials & Interfaces*, 2024, **16**, 31922-31935.
29. J. Goding, A. Gilmour, P. Martens, L. Poole-Warren and R. Green, *Advanced Healthcare Materials*, 2017, DOI: 10.1002/adhm.201601177, 1601177-n&#x1601172F;a.
30. U. A. Aregueta-Robles, P. J. Martens, L. A. Poole-Warren and R. A. Green, *Journal of Polymer Science, Part B: Polymer Physics*, 2018, **56**, 273-287.
31. R. S. Rogers and H. Nishimune, *Matrix Biology*, 2017, **57-58**, 86-105.
32. C. Legay and A. Dobbertin, *Neuroscience Letters*, 2020, **735**.
33. U. A. Aregueta Robles, F. Bartlett-Tomasetig and L. A. Poole-Warren, *Biofabrication*, 2023.

View Article Online
DOI: 10.1039/D5TB02475G

Data for this article, including high-resolution images, NMR spectra, and processed data are available at Science Data Bank at https://doi.org/10.57760/sciencedb.31214.

Restricted Access: You may request access to the data files in this upload, provided that you fulfil the conditions below. The decision whether to grant/deny access is solely under the responsibility of the data depositor. The applicant shall provide the name, organization information and purpose.